Journal of Anatomy

J. Anat. (2010) **216**, pp724–731 doi: 10.1111/j.1469-7580.2010.01225.x

Collagen fibril morphology and mechanical properties of the Achilles tendon in two inbred mouse strains

S. Rigozzi,[1] R. Müller[1] and J. G. Snedeker[1,2]

[1]*Institute for Biomechanics, ETH Zurich, Zurich, Switzerland*
[2]*Orthopedic Research Laboratory, University of Zurich, Balgrist, Zurich, Switzerland*

Abstract

The relationship between collagen fibril morphology and the functional behavior of tendon tissue has been investigated in numerous experimental studies. Several of these studies suggest that larger fibril radius is a primary determinant of higher tendon stiffness and strength; others have shown that factors apart from fibril radius (such as fibril–fibril interactions) may be critical to improved tendon strength. In the present study, we investigate these factors in two inbred mouse strains that are widely used in skeletal structure–function research: C57BL/6J (B6) and C3H/HeJ (C3H). The aim was to establish a quantitative baseline that will allow one to assess how regulation of tendon extracellular matrix architecture affects tensile mechanical properties. We specifically focused on collagen fibril structure and glycosaminoglycan (GAG) content – the two primary constituents of tendon by dry weight – and their potential functional interactions. For this purpose, Achilles tendons from both groups were tested to failure in tension. Tendon collagen morphology was analyzed from transmission electron microscopy images of tendon sections perpendicular to the longitudinal axis. Our results showed that the two inbred strains are macroscopically similar, but C3H mice have a higher elastic modulus ($P < 0.05$). Structurally, C3H mice showed a larger collagen fibril radius compared to B6 mice (96 ± 7 nm and 80 ± 10 nm respectively). Tendons from C3H mice also showed smaller specific fibril surface (0.015 ± 0.001 nm nm^{-2} vs. 0.017 ± 0.003 nm nm^{-2} in the B6 tendons, $P < 0.05$), and accordingly a lower concentration of GAGs (0.60 ± 0.07 μg mg^{-1} vs. 0.83 ± 0.11 μg mg^{-1}, $P < 0.05$). As in other studies of tendon structure and function, larger collagen fibril radius appears to be associated with stiffer tendon, but this functional difference could also be attributed to reduced potential surface area exchange between fibrils and the surrounding proteoglycan-rich matrix, in which the hydrophilic GAG side chains may promote inter-fibril sliding. This study provides an architectural and functional baseline for a comparative murine model that can be used to investigate the genetic regulation of tendon biomechanics.

Key words Achilles tendon; biomechanics; collagen fibrils morphology; glycosaminoglycans; inbred strain.

Introduction

The relationship between the distribution of collagen fibrils and functional behavior of tendon has been investigated in numerous experimental studies. Several of these suggest that an increased fibril radius is a primary determinant of improved tendon stiffness and strength (Parry, 1988; Battaglia et al. 2003; Liao & Vesely, 2003; Lin et al. 2004). However, more recent studies have shown that despite a generally smaller fibril radius in healing tendon, it gains strength with an increase in the fibril area fraction, and that factors apart from fibril radius may be critical to improved tendon strength (Battaglia et al. 2003). Consistent with this concept, an earlier study indicated that Achilles tendons of growth differentiation factor 5 (GDF-5) deficient mice showed drastically reduced functional performance, although composed of nearly normal fibril radius distributions and fibril area fractions (Mikic et al. 2001). Generally these studies indicate that biochemical deficiencies in the non-collagenous extracellular matrix (ECM) may be a primary causative factor in certain tendon pathologies.

Two main classes of extracellular macromolecules make up the tendon matrix: proteoglycans (PGs), which play a complex role in force transmission and maintenance of tendon tissue structure (Reed & Iozzo, 2002; Rigozzi et al.

Correspondence
Prof. Jess G Snedeker, University of Zurich, Balgrist, Forchstrasse 340, CH – 8008 Zurich, Switzerland. T: + 41 44 3863755; F: +41 44 386 1109; E: jsnedeker@research.balgrist.ch

Accepted for publication *18 February 2010*
Article published online *23 March 2010*

2009), and collagen fibrils. Studies that have investigated the relationship between structural and mechanical properties have generally focused on one major component, either collagen or proteoglycans (PG), with studies focusing on collagen fibril morphology being more common. Some of the earliest studies have related collagen fibril morphology and mechanical properties (Parry et al. 1978; Parry, 1988; Derwin & Soslowsky, 1999), and these suggest that the ability of tendon to bear high stress is positively related to the percentage of large fibrils in the tissue, whereas creep-inhibition properties are related to the percentage of small fibrils. These studies suggest that tendon is thus able to fulfill its specific functional demands by regulating an appropriate collagen architecture. On the other hand, various studies report that a high concentration of negatively charged PG side chains – the glycosaminoglycans (GAGs) – is related to an increased osmotic pressure and enhanced tissue hydration (Yoon & Halper, 2005). This tissue hydration could separate individual fibril bundles and minimize shear stress as fibrils move relative to one another (Berenson et al. 1996). In other words, PGs may lubricate the structure at the molecular level, facilitate inter-fibril slippage, and thus make the tissue more compliant.

In the present study, we evaluated the ultrastructural and mechanical properties of the Achilles tendon in the two inbred mouse strains, C57BL/6J (B6) and C3H/HeJ (C3H). Adult B6 and C3H mice have a similar body size and weight and their skeletons are similarly sized, but they show morphologically distinct skeletal traits (Jepsen et al. 2003). Despite differences in adult peak bone density and whole bone cross-sectional area, they have similar bone mechanical properties at the structural level (Kodama et al. 2000). We hypothesized that, as with bone, these two genotypes would show differences in tendon architecture while exhibiting similar macroscopic mechanical behavior – and thus provide a useful comparative (genetic) model for investigating tendon structure–function. In quantifying tendon structure, we focused on defining the collagen fibril morphology in terms of both fibril radius and the potential for fibril-to-fibril interactions. This allows one to extract information about the relative functional contribution of not only the collagen, but also other macromolecules such as the PG decorin, which attaches to the surface of the collagen fibrils at regular intervals (Scott, 1988). The aim of this study was thus to define an architectural and functional baseline for the comparison of two inbred mouse strains to serve as a model for a genetic basis of tendon structure and function.

Materials and methods

Animal model

This study was reviewed and approved by the local and state authorities for all levels of animal investigation. We used two inbred mouse strains with markedly different skeletal phenotypes, where B6 represents the low bone mass and C3H represents the high bone mass phenotype (Akhter et al. 1998; Turner et al. 2000; Jepsen et al. 2003; Tommasini et al. 2005; Voide et al. 2008). Ten B6 and 10 C3H female mice were purchased from the Harlan breeding facility (Horst, The Netherlands). Mice were sacrificed by CO_2 inhalation at 19 weeks of age. The animals were then stored at −20 °C and thawed at room temperature just before dissection of the Achilles tendon. Twenty Achilles tendons were harvested from each of the two strains.

Collagen fibril structure analysis

The tendon connected to the soleus muscle was dissected and fixed in a solution of 2% glutaraldehyde for 30 min and rinsed three times with 0.1 M cacodylate buffer (pH 7.4). After fixation, tendons were postfixed with 2% osmium oxide for 30 min and then rinsed three times in distilled water. The samples were stained with ethanolic uranyl acetate (2% uranyl acetate/50% ethanol) overnight and then rinsed twice with distilled water. Dehydration was continued through a cold (4 °C), graded ethanol series. The tendons were infiltrated and embedded with propylene oxide in a fresh mixture of Epon and ethanol, and polymerized for 2 days in the oven at 60 °C.

Sections of 50–70 nm thickness were cut perpendicular to the longitudinal axis of the tendon with a diamond knife mounted on an ultramicrotome (Reichert Ultracut E, Wetzlar, Germany) Sections taken approximately 1 mm proximal to the calcaneous attachment were mounted on Butvar-coated 1×2 mm slot grids, and contrasted with 2% uranyl acetate and lead citrate according to the method of Reynolds (1963). The region of interest (ROI) was identified at ×5000 magnification. Using a transmission electron microscope (TEM), seven micrographs per tendon were taken at a final magnification of ×40 000 (Fig. 1). The 14 animals thus yielded a total of 98 micrographs at 100 kV.

A script was written in MATLAB (The MathWorks, version 7.4) to automatically quantify morphological parameters, as schematized in Fig. 2. The original image was automatically calibrated, treated with a Gauss filter (width, $\sigma = 1.2$; support, $s = 3$ voxels), and a threshold was set according to the algorithm of Trussell (1979) to give a binary image that was stored and used to measure the geometric parameters of the fibrils. The measured parameters described below can be divided in two groups: classic parameters widely described for collagen morphology characterization (collagen fibril radius, collagen area fraction), and newly introduced morphometric parameters describing the potential for lateral interactions between the collagen fibrils (interfibrillar distance, specific fibril surface, fibril contact area). The *collagen fibril radius* of each collagen fibril was represented by the minor collagen radius, to avoid any error due to oblique fibril angle in relation to the image plane. Additionally, the fibril radii of the seven images from each animal were cumulatively summed to give an overall indication of the distribution. The cumulative curves were shown to give a supplementary overall indication of the distribution within the two strains. *Collagen area fraction* was defined as the total fibril area in the image divided by the total image area (yielding a dimensionless parameter). The *interfibrillar distance* was defined as the mean spacing between fibrils expressed in nm. This value was calculated by applying a distance transform on the gap between the fibrils (Hildebrand & Rüegsegger, 1997), resulting in the average

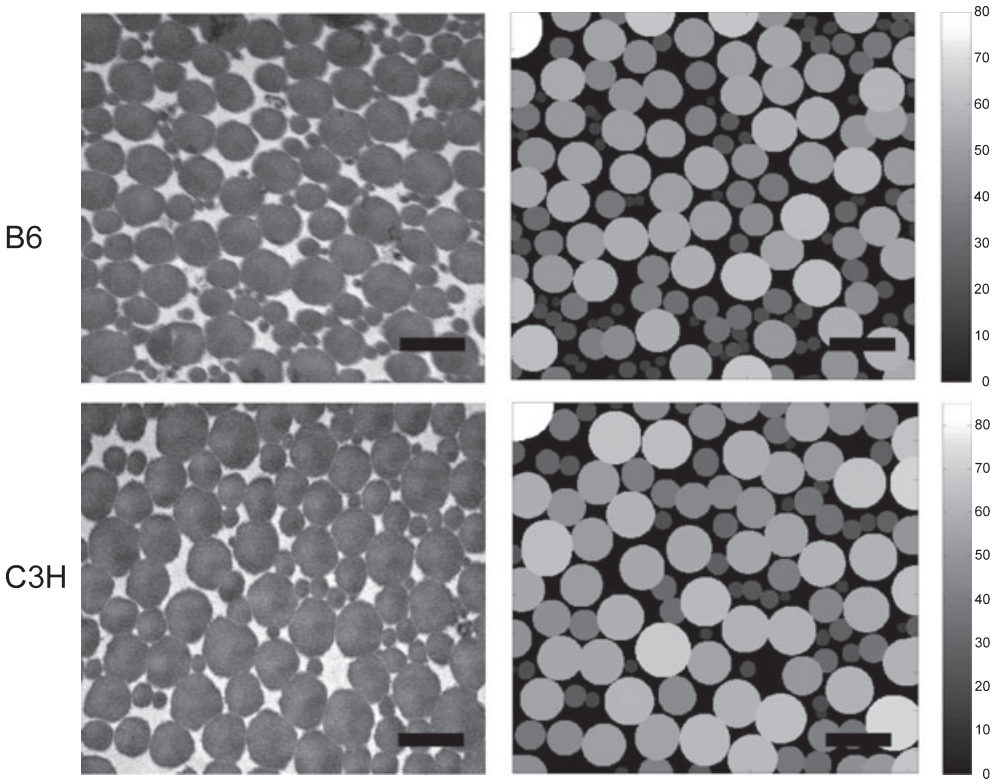

Fig. 1 Representative transmission electron micrograph for the two inbred strain, B6 and C3H, and its binarized reconstruction on the right. The binarized reconstruction is processed to calculate the fibril radius, the collagen area fraction, the interfibrillar distance, the specific fibril surface and the fibril contact area. The color bar indicates the pixel size of the fibril radius that is converted to nm. The black bar indicates 400 nm.

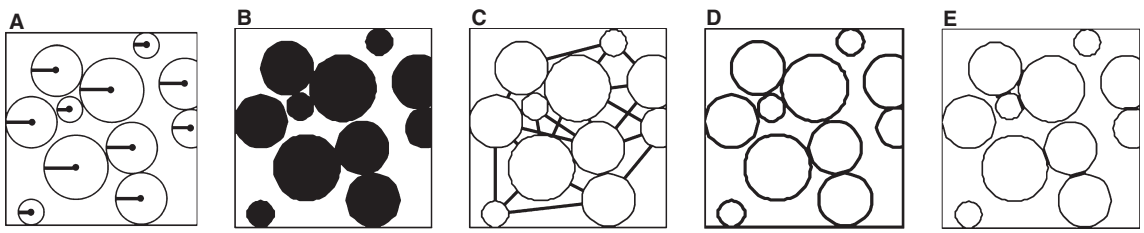

Fig. 2 Schematic representation of the morphological parameters measured with the automatic script. (A) Fibril radius, (B) collagen area fraction, (C) interfibrillar distance, (D) specific fibril surface, (E) fibril contact area.

distance between a given fibril and all neighboring fibrils that can be connected by an uninterrupted line segment (Fig. 2C). The *specific fibril surface*, expressed in nm nm^{-2}, is a normalized value consisting of the total perimeter of all fibrils within a given image divided by the total image area (Fig. 2D). The *fibril contact area* is defined as the percentage of the total fibril perimeter that is in contact with neighboring fibrils (Fig. 2E). Two fibrils are considered in contact if the total perimeter of each cannot be distinguished as an isolated circle on a binary image. The exchange area between the collagen fibrils and the outer ECM is calculated by applying a Canny filter on the filtered image (Pantelic et al. 2007). The Canny filter detects the edges of the fibrils by applying two thresholds to the gradient: a high threshold for low edge sensitivity and a low threshold for high edge sensitivity. The filter starts from the low sensitivity and then increases it to include connected edge pixels from the high sensitivity result to fill in gaps in the detected edges.

GAG analysis

To relate the morphological measures of potential for fibril-to-fibril interactions to PG content, we assessed GAG content. Tendons were weighed and digested for 16 h with 500 U mL^{-1} papain solution in buffer (0.1 M disodium hydrogen phosphate, 0.01 M EDTA disodium salt, 14.4 mM L-cysteine) at 60 °C. GAG content was determined spectrophotometrically (Cary 50, Varian; Zug, Switzerland) at 525 nm following binding to dimethylmethylene blue dye (DMMB) (Farndale et al. 1986) using chondroitin sulfate as the standard.

Cupromeronic blue dye (CB) was used to visualize GAG architecture with TEM according to reported studies (Haigh & Scott, 1986; Liao & Vesely, 2004). Briefly, freshly dissected Achilles tendons connected to the soleus muscle were stained overnight with 1% CB in 0.2 M acetate buffer (pH 5.6). After rinsing in the same solution without CB, samples were immersed in 0.5% Na_2WO_4 in buffer for 1 h and then overnight in 0.5% Na_2WO_4 in 30% ethanol. To stain the collagen fibrils, samples were stained with 1% uranyl acetate and fixed with the Reynolds technique as mentioned above (Reynolds, 1963).

Biomechanical testing

Mechanical tests were performed with a universal testing machine (Zwick 1456; Ulm, Germany). Tendons were preconditioned with 10 cycles of 0–10% nominal strain before ramp loading to failure at 10 mm min^{-1}, as described earlier (Rigozzi et al. 2009). Force displacement data from the ramp-to-failure test were analyzed for ultimate stress, failure strain, and elastic (E) modulus.

Statistical analysis

A Lilliefors test was used to determine whether data were adequately fitted to a normal distribution. For normally distributed data, an unpaired *t*-test was used to test the significance of the two strains on measured morphological and mechanical parameters. Otherwise, a Wilcoxon rank sum test was used to test significance between the strains. A *P*-value < 0.05 was considered to be significant.

Two-sample Kolmogorov–Smirnov testing was used to compare the distribution of the collagen fibril mean radii between the cumulative curves of the two inbred mouse strain. The distributions were considered significantly different for *P*-values < 0.05.

Results

Collagen fibril structure analysis

Images from the two inbred strains were compared; the results are summarized in Table 1. Results show that C3H mice have a significantly larger mean fibril radius than B6 mice, whereas the collagen area fraction of the ECM and the lateral spacing between fibrils can be considered the same for both groups. Specific fibril surface was significantly higher in the B6 strain, but effective fibril contact area was statistically similar. Figure 3 shows cumulative distribution curves for fibril radii for each mouse. The curves for the B6 strain have a steeper slope, indicating that they contain more small-radius fibrils than the C3H. There was a statistically significant inter-strain difference for the curves.

GAG analysis

The GAG assay indicated a statistically significant difference in GAG concentration (chondroitin sulfate and dermatan sulfate); for B6 0.83 ± 0.11 μg mg^{-1} and for C3H 0.60 ± 0.07 μg mg^{-1} ($P \leq 0.05$). Representative transmission electron micrographs of the longitudinal sections of the two inbred strain are shown in Fig. 4.

Biomechanical testing

During mechanical testing, all tendons failed in the midsubstance. Video analysis revealed no slippage at the clamp. The mechanical parameters are summarized in Table 2. Both groups had a similar tendon length (5.5 ± 0.7 for the B6 and 5.5 ± 0.6 mm for the C3H), and cross-sectional area (0.49 ± 0.10 mm^2 for the B6 and 0.54 ± 0.14 mm^2 for the C3H). The C3H group exhibited a median E-modulus of 140 MPa, whereas B6 was significantly lower at 123 MPa ($P < 0.05$). No statistically significant difference in either mean failure strain ($\varepsilon_{B6} = 36 \pm 17$ % $\varepsilon_{C3H} = 33 \pm 9$ %) or mean ultimate stress ($\sigma_{B6} = 10 \pm 4$ MPa $\sigma_{C3H} = 13 \pm 4$ MPa) was observed.

Assessing structure and function

Tables 1 and 2 summarize all the measured values of the two strains of inbred mice. The two groups had similar gross anatomical characteristics, with no statistical difference seen in cross-sectional area, or tendon length at the given preload. No differences were observed in stiffness, maximal force or maximal strain. Mechanically, the C3H showed a statistically higher elastic modulus than B6 ($P < 0.05$). Ultimate stresses were higher in the C3H, but this was not statistically significant.

Data demonstrated morphological differences at the collagen fibril level. The C3H group had significantly larger mean fibril radii and a lower fibril perimeter than the B6, whereas the B6 group showed a higher specific fibril surface ($P < 0.05$). Other morphological parameters such as

Table 1 Summary of measured morphological parameters measured for B6 and C3H mice.

	Mean radius (nm)	Collagen area fraction (%)	Interfibrillar distance (nm)	Specific fibril surface (nm nm^{-2})	Fibril contact area (%)
C57BL/6	79.7 ± 9.7*	72.5 ± 3.8	10.8 ± 1.6	0.017 ± 0.003*	33.0 ± 4.2
C3H/HeJ	95.7 ± 7.0*	73.1 ± 3.0	10.9 ± 2.1	0.015 ± 0.001*	34.5 ± 2.5

*Statistically significant for *P*-value < 0.05.

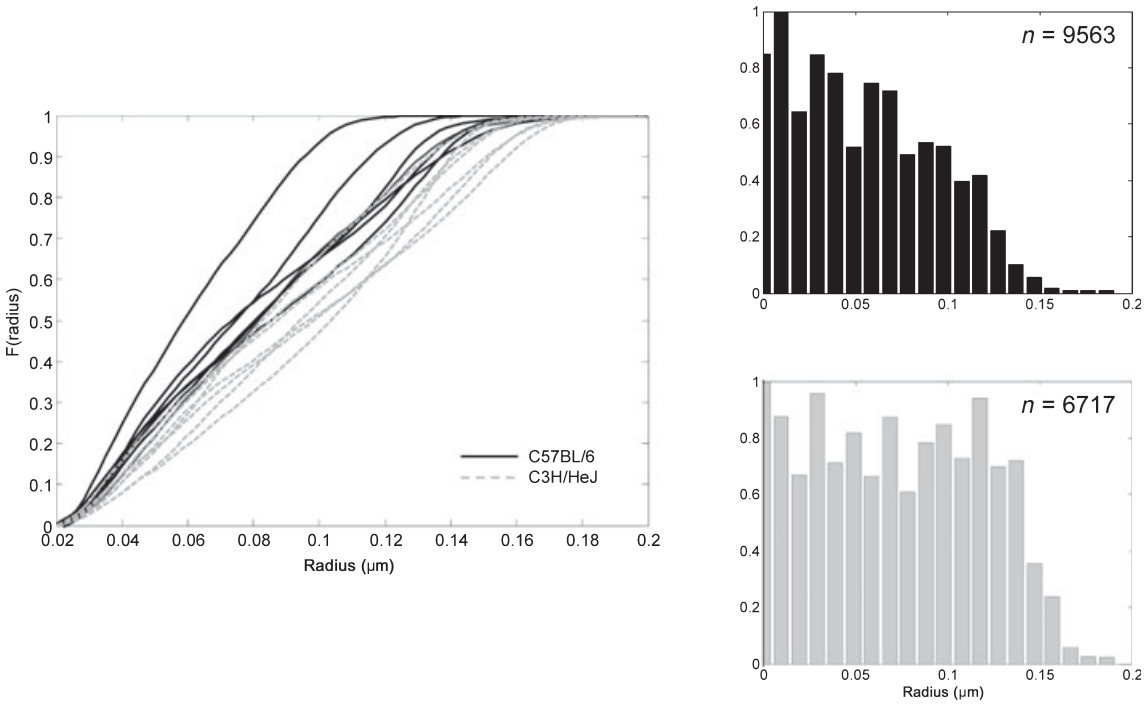

Fig. 3 Cumulative distribution curves for B6 and C3H mice. B6 generally contain a majority of small fibrils, whereas C3H have a more uniformly distributed fibril radius. Histograms of the collagen fibril distribution for both groups. *n* is the total number of fibrils.

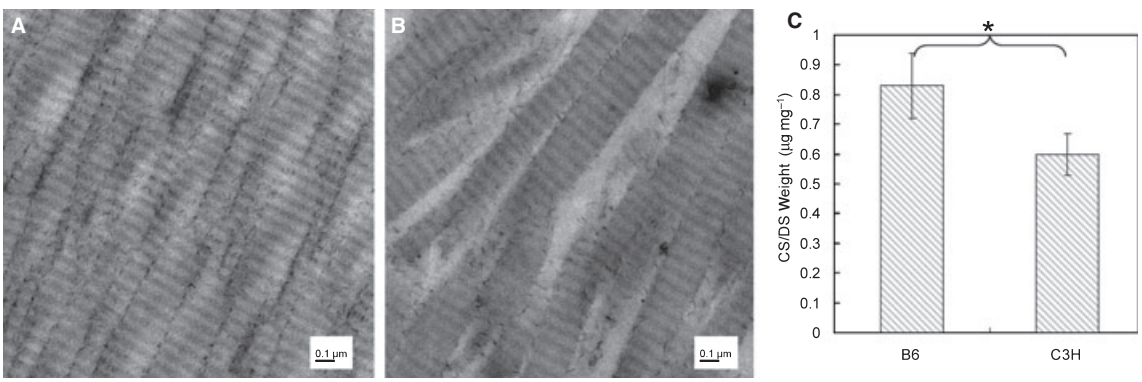

Fig. 4 Representative transmission electron micrograph of a longitudinal section of the Achilles tendon for (A) B6 and (B) C3H at a magnification of ×53 000. The black lines between the fibrils are the stained GAGs. (C) Means and standard deviations of sulfated GAG content in the two groups. *Statistically significant for *P*-value ≤ 0.05.

collagen area fraction, interfibrillar distance and fibril contact area did not show statistical differences.

Thus, the B6 group tendons were similarly sized but generally less stiff than the C3H tendons, which had fewer, larger collagen fibrils and smaller potential for lateral interactions between fibrils or between fibrils and the other components of the ECM.

Discussion

Tendon stiffness is central to proper function (Lichtwark & Wilson, 2008), and how tendon structure relates to function is critical to understanding tendon pathology (Magnusson et al. 2002; Riley, 2004; Pufe et al. 2005; Smith et al. 2008) as well as in developing strategies for healing (Battaglia et al. 2003; Aslan et al. 2008). In this work, we introduce a potentially useful comparative tendon structure–function model in two inbred mouse strains by describing the collagen morphology and the corresponding mechanical properties of the soleus tendon. The mechanical properties of this load-bearing, elastic tendon were considered with respect to the observed morphology of the collagen fibrils, where it was found that tendons with larger diameter collagen fibrils

Table 2 Summary of the measured mechanical parameters for B6 and C3H. The E-modulus is showed as median (first quartile; third quartile).

	Structural data					Material data	
Groups	Lo (mm)	Area (mm^2)	Force max (N)	Failure strain (%)	Stiffness ($N\ mm^{-1}$)	Ultimate stress (MPa)	E modulus (MPa)
C57BL/6	5.5 ± 0.7	0.54 ± 0.14	6.0 ± 2.3	36 ± 17	52 ± 36	10.4 ± 3.9	123 (52;203)*
C3H/HeJ	5.5 ± 0.6	0.49 ± 0.10	6.4 ± 1.8	33 ± 9	75 ± 28	13.0 ± 3.7	140 (112;198)*

*Statistically significant for *P*-value < 0.05.

and lower specific fibril surface also exhibited a higher elastic modulus.

Previous studies have investigated the morphology of collagen fibrils from cross-sectional area TEM images. Some have focused on the collagen radius in ruptured tendons (Moeller et al. 1995; Magnusson et al. 2002), and some on the changes to the collagen during collagen assembly (Chapman, 1989). Others have focused on the collagen fibril diameters in different anatomical structures and their relationship to corresponding function (Rumian et al. 2007). In all of these studies, fibril morphology has been described primarily in terms of fibril diameter. In the current study we introduce new morphological parameters that permit insight into potential fibril–fibril interactions and fibril–non-fibrillar matrix interactions such as the interfibrillar distance between the fibrils, the specific fibril surface, and direct fibril–fibril contact (see Fig. 2 and Table 1). These parameters not only give a more thorough description of the collagen morphology, but may also offer better insight into structure–function relationships.

Studies analyzing structure–function in tendons usually consider the functional relevance of collagen fibril morphology and proteoglycan content separately, and thus neglect potential functional interplay between collagen and PGs. By expanding our quantification of collagen fibril morphology to include descriptors relevant to fibril–fibril interactions, we have attempted here to bridge the conceptual treatment of these two components, which are known to influence each other during tissue formation (Pins et al. 1997; Graham et al. 2000; Yoon & Halper, 2005), and which may influence their mechanical functions (Cribb & Scott, 1995; Redaelli et al. 2003; Robinson et al. 2005; Liao & Vesely, 2007; Rigozzi et al. 2009).

Our mechanical and morphological comparison between B6 and C3H showed that despite very similar collagen area fractions, C3H tendons are considerably stiffer than B6 tendons. This could be attributed to larger fibril size; the B6 mouse strain has Achilles tendons constituted by smaller fibrils. Alternatively, the lower modulus in the B6 mice may also be explained partly by greater collagen fibril surface area and fibril-hydrated ECM interactions. Collagen fibrils are densely linked to hydrophilic PG chains where their surface is in contact with the matrix, and these chains may therefore facilitate relative movement of the fibrils through the matrix (Wren & Carter, 1998). Considering that the collagen fibrils are linked to PG chains where their surface is in contact with the matrix, we surmise that the amount of PGs present in the tendon is directly correlated to the relative fibril surface area. Our results described in Tables 1 and 2 show that C3H mice, which have a larger E modulus and lower total fibril surface area, also have a lower measured concentration of sulfated groups (DS and CS). Thus, less PG may be associated with a higher elastic modulus. As discussed below, this is in contrast with other studies that invoke the structure–function model that the PGs may actually have interconnect neighboring fibrils (Scott, 1980, 1988; Raspanti et al. 1997; Scott & Thomlinson, 1998), transfer forces between them (Scott, 2003; Liao & Vesely, 2007), and lead to stiffer tendons (Redaelli et al. 2003).

Given comparable macroscopic/microscopic tendon architecture in the two evaluated inbred strains, classic composite theory suggests that the observed similarity in collagen area fraction (e.g. effective collagen content) in both groups would yield a similar mechanical response in terms of elastic modulus and failure stress (Ault & Hoffman, 1992a,b; Wren & Carter, 1998). In fact, the C3H demonstrated significantly higher elastic modulus, but a similar failure behavior. This suggests that a more sophisticated model of tendon structure-function is required.

More elaborate models of tendon structure–function have been introduced, taking into account fibril–fibril interactions through matrix cross-linking by proteoglycan GAG sidechains (Redaelli et al. 2003; Ciarletta et al. 2008). In the present study, the close similarity in both mean interfibrillar distance and fibril–fibril contact area suggests that there would be no relative advantage in either group with regard to direct fibril–fibril interactions (lateral force transfer between fibrils) that might promote a higher elastic modulus of the C3H tendons. In fact, according to this model the higher relative GAG content in the B6 mice should confer stiffer tendon properties, which is in direct contrast to our experimental observations. Thus the present study suggests that tendon structure–function is also not adequately described by the theoretical framework of proteoglycan-mediated collagen fibril load sharing. This lends support to our recent studies indicating that GAG side chains of small leucine-rich proteoglycans do not play a dominant role in

tensile mechanics of the tendon midsubstance (Fessel & Snedeker, 2009; Rigozzi et al. 2009).

Until now, most studies investigating GAG-mediated fibril–fibril interactions have relied on either PG knock-out mice (Robinson et al. 2005) or enzyme digestion of the PG side chains (Koob, 1989; Lujan et al. 2007; Fessel & Snedeker, 2009; Rigozzi et al. 2009). Cross-sectional comparisons of structure and function in two different inbred wild-type strains can complement such studies by avoiding problematic limitations inherent in these approaches. For instance, a 'targeted' enzymatic digestion of the GAG component does not guarantee that another component will not be affected and show secondary effects, such as swelling of the collagen fibers (Pek et al. 2004). Also, in studies with knock-out mice, the lack of a certain gene does not ensure that redundant processes will not compensate its loss and restore function (Robinson et al. 2005; Wang, 2006).

Our choice of inbred mouse strains with regard to a structure–function baseline in tendon is rooted in a history of studies investigating bone morphology of different inbred strains to correlate them with their mechanical response (Akhter et al. 1998; Turner et al. 2000; Jepsen et al. 2003; Tommasini et al. 2005; Voide et al. 2008). B6 and C3H have been identified as a model to study the genetic factors in osteoporosis (Beamer et al. 1999). As tendon to bone healing remains a pressing clinical challenge (Thomopoulos et al. 2003; Kovacevic & Rodeo, 2008), this model may be enlarged to permit a broader view of how these two connective tissues influence each other.

It should be noted that our previous studies have revealed that heterogeneous histological structure (e.g. tendon regions nearer to the bone and muscle insertions) has important implications with regard to the mechanical influence of proteoglycans on tensile mechanics (Rigozzi et al. 2009). The aim of the present work was to focus on a specific subregion of the tendon with more homogeneous tissue architecture, in hopes of reducing the parameters considered in our structure–function analysis. While we intentionally focused the scope of the present investigation on the tendon midsubstance, quantitative investigation of the transition between tendon and muscle or tendon and bone remains an area for future work.

To conclude, inbred C3H mice have a higher elastic modulus, larger mean fibril radius, lower fibril surface area, lower GAG content, similar collagen area fractions, and similar direct fibril–fibril contact compared to B6 mice. This study thus establishes a useful baseline for further investigation of the influence of tendon morphology on tendon mechanical properties in two inbred strain populations that are increasingly used as models for orthopedic disease. This baseline forms a foundation for future studies into the genetic regulation of tendon modeling and remodeling. It will also aid in the interpretation of existing studies that have employed selective chemical degradation of tendon ECM components, and transgenic animal models used to understand how tendon derives its mechanical characteristics from its basic architecture and biochemical composition.

Acknowledgements

This work was supported through BEST Bioengineering Cluster at ETH Zurich (Switzerland) and the EU grant LHSB-CT-2003-503161 (Genostem).

References

Akhter MP, Cullen DM, Pedersen EA, et al. (1998) Bone response to in vivo mechanical loading in two breeds of mice. *Calcif Tissue Int* **63**, 442–449.

Aslan H, Kimelman-Bleich N, Pelled G, et al. (2008) Molecular targets for tendon neoformation. *J Clin Invest* **118**, 439–444.

Ault HK, Hoffman AH (1992a) A composite micromechanical model for connective tissues: part I – Theory. *J Biomech Eng* **114**, 137–141.

Ault HK, Hoffman AH (1992b) A composite micromechanical model for connective tissues: part II – Application to rat tail tendon and joint capsule. *J Biomech Eng* **114**, 142–146.

Battaglia TC, Clark RT, Chhabra A, et al. (2003) Ultrastructural determinants of murine achilles tendon strength during healing. *Connect Tissue Res* **44**, 218–224.

Beamer WG, Shultz KL, Churchill GA, et al. (1999) Quantitative trait loci for bone density in C57BL/6J and CAST/EiJ inbred mice. *Mamm Genome* **10**, 1043–1049.

Berenson MC, Blevins FT, Plaas AH, et al. (1996) Proteoglycans of human rotator cuff tendons. *J Orthop Res* **14**, 518–525.

Chapman JA (1989) The regulation of size and form in the assembly of collagen fibrils in vivo. *Biopolymers* **28**, 1367–1382.

Ciarletta P, Dario P, Micera S (2008) Pseudo-hyperelastic model of tendon hysteresis from adaptive recruitment of collagen type I fibrils. *Biomaterials* **29**, 764–770.

Cribb AM, Scott JE (1995) Tendon response to tensile stress: an ultrastructural investigation of collagen:proteoglycan interactions in stressed tendon. *J Anat* **187**(Pt 2), 423–428.

Derwin KA, Soslowsky LJ (1999) A quantitative investigation of structure-function relationships in a tendon fascicle model. *J Biomech Eng* **121**, 598–604.

Farndale RW, Buttle DJ, Barrett AJ (1986) Improved quantitation and discrimination of sulphated glycosaminoglycans by use of dimethylmethylene blue. *Biochim Biophys Acta* **883**, 173–177.

Fessel G, Snedeker JG (2009) Evidence against proteoglycan mediated collagen fibril load transmission and dynamic viscoelasticity in tendon. *Matrix Biol* **28**, 503–510.

Graham HK, Holmes DF, Watson RB, et al. (2000) Identification of collagen fibril fusion during vertebrate tendon morphogenesis. The process relies on unipolar fibrils and is regulated by collagen-proteoglycan interaction. *J Mol Biol* **295**, 891–902.

Haigh M, Scott JE (1986) A method of processing tissue sections for staining with cu-promeronic blue and other dyes, using CEC techniques, for light and electron microscopy. *Basic Appl Histochem* **30**, 479–486.

Hildebrand T, Rüegsegger P (1997) A new method for the model-independent assessment of thickness in three-dimensional images. *J Microsc* **185**, 67–75.

Jepsen KJ, Akkus OJ, Majeska RJ, et al. (2003) Hierarchical relationship between bone traits and mechanical properties in inbred mice. *Mamm Genome* **14**, 97–104.

Kodama Y, Umemura Y, Nagasawa S, et al. (2000) Exercise and mechanical loading increase periosteal bone formation and whole bone strength in C57BL/6J mice but not in C3H/Hej mice. *Calcif Tissue Int* **66**, 298–306.

Koob TJ (1989) Effects of chondroitinase-ABC on proteoglycans and swelling properties of fibrocartilage in bovine flexor tendon. *J Orthop Res* **7**, 219–227.

Kovacevic D, Rodeo SA (2008) Biological augmentation of rotator cuff tendon repair. *Clin Orthop Relat Res* **466**, 622–633.

Liao J, Vesely I (2003) A structural basis for the size-related mechanical properties of mitral valve chordae tendineae. *J Biomech* **36**, 1125–1133.

Liao J, Vesely I (2004) Skewness angle of interfibrillar proteoglycan increases with applied load on chordae tendineae. *Conf Proc IEEE Eng Med Biol Soc* **5**, 3741–3744.

Liao J, Vesely I (2007) Skewness angle of interfibrillar proteoglycans increases with applied load on mitral valve chordae tendineae. *J Biomech* **40**, 390–398.

Lichtwark GA, Wilson AM (2008) Optimal muscle fascicle length and tendon stiffness for maximising gastrocnemius efficiency during human walking and running. *J Theor Biol* **252**, 662–673.

Lin TW, Cardenas L, Soslowsky LJ (2004) Biomechanics of tendon injury and repair. *J Biomech* **37**, 865–877.

Lujan TJ, Underwood CJ, Henninger HB, et al. (2007) Effect of dermatan sulfate glycosaminoglycans on the quasi-static material properties of the human medial collateral ligament. *J Orthop Res***25**, 894–903.

Magnusson SP, Qvortrup K, Larsen JO, et al. (2002) Collagen fibril size and crimp morphology in ruptured and intact Achilles tendons. *Matrix Biol* **21**, 369–377.

Mikic B, Schalet BJ, Clark RT, et al. (2001) GDF-5 deficiency in mice alters the ultrastructure, mechanical properties and composition of the Achilles tendon. *J Orthop Res* **19**, 365–371.

Moeller HD, Bosch U, Decker B (1995) Collagen fibril diameter distribution in patellar tendon autografts after posterior cruciate ligament reconstruction in sheep: changes over time. *J Anat* **187**(Pt 1), 161–167.

Pantelic RS, Ericksson G, Hamilton N, et al. (2007) Bilateral edge filter: photometrically weighted, discontinuity based edge detection. *J Struct Biol* **160**, 93–102.

Parry DA (1988) The molecular and fibrillar structure of collagen and its relationship to the mechanical properties of connective tissue. *Biophys Chem* **29**, 195–209.

Parry DA, Barnes GR, Craig AS (1978) A comparison of the size distribution of collagen fibrils in connective tissues as a function of age and a possible relation between fibril size distribution and mechanical properties. *Proc R Soc Lond B Biol Sci* **203**, 305–321.

Pek YS, Spector M, Yannas IV, et al. (2004) Degradation of a collagen–chondroitin-6-sulfate matrix by collagenase and by chondroitinase. *Biomaterials* **25**, 473–482.

Pins GD, Christiansen DL, Patel R, et al. (1997) Self-assembly of collagen fibers. Influence of fibrillar alignment and decorin on mechanical properties. *Biophys J* **73**, 2164–2172.

Pufe T, Petersen WJ, Mentlein R, et al. (2005) The role of vasculature and angiogenesis for the pathogenesis of degenerative tendons disease. *Scand J Med Sci Sports* **15**, 211–222.

Raspanti M, Alessandrini A, Ottani V, et al. (1997) Direct visualization of collagen-bound proteoglycans by tapping-mode atomic force microscopy. *J Struct Biol* **119**, 118–122.

Redaelli A, Vesentini S, Soncini M, et al. (2003) Possible role of decorin glycosaminoglycans in fibril to fibril force transfer in relative mature tendons – a computational study from molecular to microstructural level. *J Biomech* **36**, 1555–1569.

Reed CC, Iozzo RV (2002) The role of decorin in collagen fibrillogenesis and skin homeostasis. *Glycoconj J* **19**, 249–255.

Reynolds ES (1963) The use of lead citrate at high pH as an electron-opaque stain in electron microscopy. *J Cell Biol* **17**, 208–212.

Rigozzi S, Muller R, Snedeker JG (2009) Local strain measurement reveals a varied regional dependence of tensile tendon mechanics on glycosaminoglycan content. *J Biomech* **42**, 1547–1552.

Riley G (2004) The pathogenesis of tendinopathy. A molecular perspective. *Rheumatology (Oxford)* **43**, 131–142.

Robinson PS, Huang TF, Kazam E, et al. (2005) Influence of decorin and biglycan on mechanical properties of multiple tendons in knockout mice. *J Biomech Eng* **127**, 181–185.

Rumian AP, Wallace AL, Birch HL (2007) Tendons and ligaments are anatomically distinct but overlap in molecular and morphological features – a comparative study in an ovine model. *J Orthop Res* **25**, 458–464.

Scott JE (1980) Collagen – proteoglycan interactions. Localization of proteoglycans in tendon by electron microscopy. *Biochem J* **187**, 887–891.

Scott JE (1988) Proteoglycan-fibrillar collagen interactions. *Biochem J* **252**, 313–323.

Scott JE (2003) Elasticity in extracellular matrix 'shape modules' of tendon, cartilage, etc. A sliding proteoglycan-filament model. *J Physiol* **553**, 335–343.

Scott JE, Thomlinson AM (1998) The structure of interfibrillar proteoglycan bridges ('shape modules') in extracellular matrix of fibrous connective tissues and their stability in various chemical environments. *J Anat* **192**(Pt 3), 391–405.

Smith MM, Sakurai G, Smith SM, et al. (2008) Modulation of aggrecan and ADAMTS expression in ovine tendinopathy induced by altered strain. *Arthritis Rheum* **58**, 1055–1066.

Thomopoulos S, Williams GR, Gimbel JA, et al. (2003) Variation of biomechanical, structural, and compositional properties along the tendon to bone insertion site. *J Orthop Res* **21**, 413–419.

Tommasini SM, Morgan TG, van der Meulen M, et al. (2005) Genetic variation in structure-function relationships for the inbred mouse lumbar vertebral body. *J Bone Miner Res* **20**, 817–827.

Trussell HJ (1979) Picture Thresholding Using an Iterative Selection Method – Comments. *IEEE Trans Syst Man Cybern* **9**, 311–311.

Turner CH, Hsieh YF, Müller R, et al. (2000) Genetic regulation of cortical and trabecular bone strength and microstructure in inbred strains of mice. *J Bone Miner Res* **15**, 1126–1131.

Voide R, van Lenthe GH, Muller R (2008) Differential effects of bone structural and material properties on bone competence in C57BL/6 and C3H/He inbred strains of mice. *Calcif Tissue Int* **83**, 61–69.

Wang JH (2006) Mechanobiology of tendon. *J Biomech* **39**, 1563–1582.

Wren TA, Carter DR (1998) A microstructural model for the tensile constitutive and failure behavior of soft skeletal connective tissues. *J Biomech Eng* **120**, 55–61.

Yoon JH, Halper J (2005) Tendon proteoglycans: biochemistry and function. *J Musculoskelet Neuronal Interact* **5**, 22–34.